

Research Article

Variations of the Reference Evapotranspiration and Aridity Index Over Northeast China: Changing Properties and Possible Causes

Liguo Cao  and Zhengchao Zhou

School of Geography and Tourism, Shaanxi Normal University, Xi'an 710119, China

Correspondence should be addressed to Liguo Cao; lgcaonju@126.com

Received 17 March 2019; Revised 5 May 2019; Accepted 4 June 2019; Published 4 July 2019

Academic Editor: Panagiotis Nastos

Copyright © 2019 Liguo Cao and Zhengchao Zhou. This is an open access article distributed under the Creative Commons Attribution License, which permits unrestricted use, distribution, and reproduction in any medium, provided the original work is properly cited.

Temporal and spatial variations in reference evapotranspiration (ET_0) and aridity index (AI) can be used as important indexes for understanding climate change and its effects on ecosystem stability. Thus, in this work, we comprehensively investigated 71 meteorological stations in Northeast China from 1965 to 2017 to analyze the spatial-temporal variation and trend of ET_0 and AI using the nonparametric Mann-Kendall test, the linear regression, and the Morlet wavelet methods. The results elucidated that ET_0 for Northeast China as a whole exhibited a decrease at a rate of -1.97 mm/yr, AI declined at a rate of -0.01 /yr during 1965–2017, and approximately 94% stations showed a decrease trend. Spatially, the high values of AI and ET_0 were primarily at the western part of the study area except for the Heilongjiang province, and the stations showing low values were mainly distributed in the central and eastern part. The decreasing trends for AI were more obvious in the eastern part compared with the western part over the study region. The abrupt changes in AI occurred in 2005 and 2007, whereas only one abrupt change for ET_0 occurred in 1995. For annual ET_0 , there were periods of 3, 7, 11, and 15 yr, and there existed periods of 1, 7, 11, and 13 yr for annual AI. The correlation coefficients implied wind speed and precipitation were the dominant meteorological factors resulting in the ET_0 and AI decrease, respectively. Additionally, the change of the Indian summer monsoon index (ISMI) may also contribute to the weakened AI in the study area. Nevertheless, further investigation is still required to clarify the mechanisms for AI and ET_0 variations in the future.

1. Introduction

The Fourth Assessment Report (AR4) provided by the Intergovernmental Panel on Climate Change (IPCC) pointed that the variation of global climate could reach an unprecedented rate in the 21st century [1, 2]. Under a warming climate, especially extreme climate events, including extreme rainfall, heat waves, floods, and droughts, would occur more frequently [2]. Additionally, climate extremes can cause great economic losses in different parts of the world [3–5], and the extreme climate events were generally more significant to natural and human systems than their mean values [6]. Thus, climate extremes have already been extensively investigated, and studies in certain regions worldwide, such as Africa [7, 8], Asia [9–12], Europe

[13, 14], and North America [15, 16]. These works have come to the conclusion that the obvious changes in temperature extremes and the spatial variations in precipitation extremes are associated with the global warming. Additionally, reference evapotranspiration (ET_0), defined as the potential evapotranspiration of a hypothetical surface of green grass of uniform height, was one of the most important hydrological variabilities for agricultural irrigation and regional hydrologic cycle [17–19], which was a significant hydrological process for water cycle. Therefore, better understanding of the changes of ET_0 was a major component in local hydrological research [20]. A majority of studies have verified the effect of climate variation on ET_0 and obtained fruitful results. The ET_0 showed a decreasing trend in all seasons, particularly in Northwest and southeast China during

1954–1993 [21], which could be attributed to the sunshine, solar radiation, and wind speed variations. Similarly, it was found that global ET_0 decreased at a rate roughly between -1 and -5 mm/yr [22–24], and the same trends of ET_0 were also found in Taoer River Basin, Yangtze River Basin, and Tibetan Plateau [25–27]. Nevertheless, it was reported that the aridity index (AI), frequently used to predict model scenarios that assess the extreme dry events, would benefit some agricultural areas [28], but AI has not been extensively employed except for Northwest China [20] and part of Tibetan Plateau [28], and the obtained results displayed that AI had a similar decreasing trend in Northwest China and significantly decreased by 0.04/10yr in the central and eastern part of Tibetan Plateau from 1960 to 2012.

Northeast China located in high latitudes is a sensitive area of climate change, especially in the central and western regions in the way of rain, and is also an important area of grain production in China. Therefore, for the purpose of studying the characteristics of change of AI and ET_0 in northeast of China from 1965 to 2017, we collected the long-term and available daily meteorological data. This paper aimed to provide scientific basis for decision making regarding rational planning of regional agricultural production and evaluating water resources, by analyzing the spatial and temporal characteristics of ET_0 and AI, which could play a vital role in understanding the effect of global warming over the study region.

2. Materials and Methods

In this section, we firstly give some essential information, such as natural conditions in the study region and dataset regarding the selected meteorological stations. Secondly, equations for calculating ET_0 and AI that have been extensively used were described in detail. Thirdly, in order to better analyze the characteristic of temporal variations of ET_0 and AI in Northeast China, the Mann–Kendall (M-K) method was introduced for assessing the temporal data trend and abrupt change in AI and ET_0 . Meanwhile, the method of Morlet wavelet was given and described, which was applied to evaluate the ET_0 and AI periodicity change.

2.1. Study Area. Northeast China ($38^{\circ}40'–53^{\circ}34'N$ and $115^{\circ}05'–135^{\circ}02'E$) is a geographical region of China (Figure 1). It mainly includes three administrative regions: Heilongjiang province, Jilin province, and Liaoning province, with a total area of around 1.24×10^6 km². Northeast China is a major manufacturing base for agriculture, forestry, grassland farming, and industry. The study region belongs to continental monsoon climate, and it is a relatively sensitive region of variations in climate under global climate models [29]. The annual mean temperature is from 4.7 to 10.7°C, with seasonal average temperature ranging from 14.7 to 23.8°C in summer and from -27.7 to 2.5°C in winter. The annual range of air temperature is even high up to 40°C. The length of time for which snow covers the ground can last for six months in certain regions [30]. The annual rainfall showed a decrease from the southeast (1000 mm) to the northwest (300 mm), and

it has an irregular seasonal precipitation distribution [31], which primarily occurred in summer and autumn.

2.2. Data Sources. In the present work, daily mean wind speed, temperature (maximum, minimum, and mean temperature), mean relative humidity, precipitation, and sunshine duration from 71 meteorological stations in Northeast China from 1965 to 2017 were obtained from the China Meteorological Information Center (Figure 1, Table 1; available at <http://data.cma.cn>). The selected stations are uniformly distributed in the study region, particularly in Jilin and Liaoning provinces. 27 stations are in the Heilongjiang province, 23 in Liaoning province, and 21 in Jilin province. The starting time of all the stations was in 1950s (Table 1). However, the time series dataset of some stations was discontinued and missing during 1950–1963; thus, we used monitoring data from 1965 to 2017 in this study. The data we used here have been subjected to strictly control the data quality and homogenization, and procedures [32–35]. Moreover, the Multivariate ENSO Index (MEI), the Pacific Decadal Oscillation (PDO), the Western North Pacific Monsoon Index (WNPMI), and the Indian Summer Monsoon Index (ISMI) were provided by the National Oceanic and Atmospheric Administration-Cooperative Institute for Research in Environmental Sciences (available at <https://www.esrl.noaa.gov/psd/>).

2.3. Reference Evapotranspiration and Aridity Index. The Penman–Monteith method is applied to estimate ET_0 from hypothetical reference grass with a height of 0.12 m, a defined surface resistance of 70 sm⁻¹, and an albedo of 0.23 [32]. The PM56 expression applied for reference evapotranspiration (ET_0) equation [32] is given as

$$ET_0 = \frac{0.408\Delta(R_n - G) + \gamma(900/(T + 273.15))U_2(e_s - e_a)}{\Delta + \gamma(1 + 0.34U_2)}, \quad (1)$$

where R_n represents the net radiation at the ground surface (MJ/(m²·d)), G stands for the ground heat flux (MJ/(m²·d)), T denotes the air temperature at a height of 2 m (m/s), γ stands for the psychrometric constant (kPa/°C), U_2 means the wind speed at 2 m height (m/s), e_s stands for the saturation vapor pressure (kPa), e_a is actual vapor pressure (kPa), and Δ stands for the slope of the saturated water-vapor pressure to air temperature curve (kPa/°C). Detailed calculation of R_n , G , γ , e_s , e_a , and Δ can be found in [36].

AI was defined for distinguishing the differences between precipitation and evapotranspiration through potential evapotranspiration [37]. The description can measure the degree of arid in certain regions. In the present work, AI can be computed as follows and it has been successfully applied to evaluate the arid degree [20]:

$$AI = \frac{(ET_0 - P)}{ET_0}, \quad (2)$$

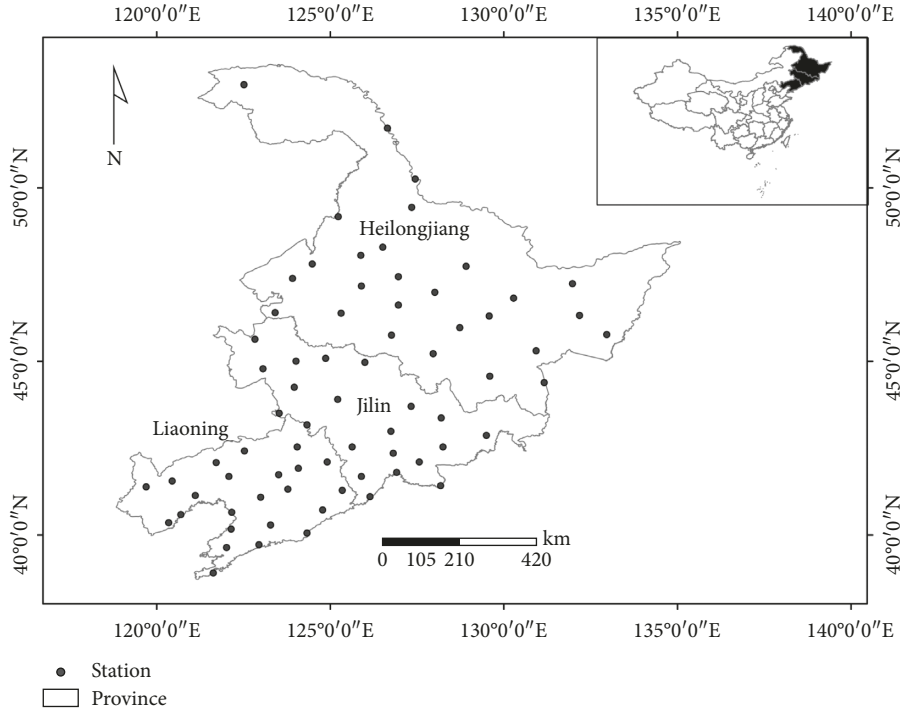


FIGURE 1: Distribution of its meteorological stations in Northeast China.

where P represents the monthly total precipitation (yearly) and ET_0 stands for the monthly reference evaporation (yearly).

2.4. Mann–Kendall Test. M-K test, famous for Kendall's tau test developed by [38, 39], is a nonparametric check for evaluating the significance of a trend for environmental data [40, 41], which was extensively adopted in studying trend detection [42, 43]. The null hypothesis H_0 is that, in a sample of data $\{x_i, i=1, 2, \dots, n\}$, x_i means independent and identically distribution. The hypothesis H_1 means a monotonic trend. The statistic S of Kendall's tau is calculated as follows:

$$S = \sum_{i=1}^{n-1} \sum_{j=i+1}^n \text{sgn}(x_j - x_i), \quad (3)$$

where x_j is the sequential data value and n means the length of data series.

$$\text{sgn}(\theta) = \begin{cases} 1, & \theta > 0, \\ 0, & \theta = 0, \\ -1, & \theta < 0. \end{cases} \quad (4)$$

Mann [39] and Kendall [38] have reported that when $n \geq 8$, the statistic S means naturally distributed with zero ($E(S) = 0$) and the variance is defined as

$$\text{Var}(S) = \frac{n(n-1)(2n+5) - \sum_{m=1}^n t_m(m-1)(2m+5)}{18}, \quad (5)$$

where t_m represents the number of ties of extent m . The standardized test Z_c is calculated by

$$Z_c = \begin{cases} \frac{S+1}{\sqrt{\text{Var}(s)}}, & S > 0, \\ 0, & S = 0, \\ \frac{S-1}{\sqrt{\text{Var}(s)}}, & S < 0, \end{cases} \quad (6)$$

where Z_c stands for the test statistics. When $|Z_c| > Z_{1-\alpha/2}$, where $Z_{1-\alpha/2}$ is the standard normal deviates and α stands for the significance for this test. Mann–Kendall index is widely applied in analyzing changes of climate data [28, 44, 45]. Temporal data show no changing trend when the value of M-K index is 0, and temporal data tend to increase when M-K index is greater than 0, whereas data tend to decrease when M-K index is less than 0.

Moreover, the M-K test was employed to test abrupt changes in AI and ET_0 in Northeast China [46].

2.5. Morlet Wavelet Method. Wavelet transform is an important method to analyze the frequency, intensity, time, and duration of the changes in a time series [27] by showing the localized time and frequency in formation. The wavelet transform has been frequently used to the fields regarding climatic change and hydrological research. In this work, according to Torrence and Compo [47], the Morlet wavelets were extensively adopted [35, 48, 49]. The Morlet wavelet function is

TABLE 1: List of stations with WMO (World Meteorological Organization) number and location.

WMO number	Station name	Province	Latitude (°N)	Longitude (°E)	Period of operation
50136	Mohe	Heilongjiang	52.97	122.52	1958–present
50353	Huma	Heilongjiang	51.72	126.65	1954–present
50468	Heihe	Heilongjiang	50.25	127.45	1959–present
50557	Nenjiang	Heilongjiang	49.17	125.23	1951–present
50564	Sunwu	Heilongjiang	49.43	127.35	1954–present
50656	Beian	Heilongjiang	48.28	126.52	1959–present
50658	Keshan	Heilongjiang	48.05	125.88	1951–present
50742	Fuyu	Heilongjiang	47.80	124.48	1957–present
50745	Qiqihaer	Heilongjiang	47.38	123.92	1951–present
50756	Hailun	Heilongjiang	47.43	126.97	1953–present
50758	Mingshui	Heilongjiang	47.17	125.90	1953–present
50774	Yichun	Heilongjiang	47.73	128.92	1956–present
50788	Fujin	Heilongjiang	47.23	131.98	1953–present
50844	Tailai	Heilongjiang	46.40	123.42	1958–present
50853	Suihua	Heilongjiang	46.62	126.97	1953–present
50854	Anda	Heilongjiang	46.38	125.32	1953–present
50862	Tieli	Heilongjiang	46.98	128.02	1958–present
50873	Jiamusi	Heilongjiang	46.82	130.28	1951–present
50877	Yilan	Heilongjiang	46.30	129.58	1959–present
50888	Baoqing	Heilongjiang	46.32	132.18	1957–present
50936	Baicheng	Jilin	45.63	122.83	1951–present
50948	Qian'an	Jilin	45.00	124.02	1957–present
50953	Haebin	Heilongjiang	45.75	126.77	1951–present
50963	Tonghe	Heilongjiang	45.97	128.73	1953–present
50968	Shangzhi	Heilongjiang	45.22	127.97	1953–present
50978	Jixi	Heilongjiang	45.30	130.93	1951–present
50983	Hulin	Heilongjiang	45.77	132.97	1957–present
54041	Tongyu	Jilin	44.78	123.07	1955–present
54049	Changling	Jilin	44.25	123.97	1953–present
54063	Sanchahe	Jilin	44.97	126.00	1953–present
54094	Mudanjiang	Heilongjiang	44.57	129.60	1951–present
54096	Suifenghe	Heilongjiang	44.38	131.17	1953–present
54142	Shuangliao	Jilin	43.50	123.53	1953–present
54157	Siping	Jilin	43.17	124.33	1951–present
54161	Changchun	Jilin	43.90	125.22	1951–present
54181	Jiaohe	Jilin	43.70	127.33	1951–present
54186	Dunhua	Jilin	43.37	128.20	1953–present
54236	Zhangwu	Liaoning	42.42	122.53	1953–present
54237	Fuxin	Liaoning	42.08	121.72	1951–present
54254	Kaiyuan	Liaoning	42.53	124.05	1955–present
54259	Qingyuan	Liaoning	42.10	124.92	1957–present
54266	Meihekou	Jilin	42.53	125.63	1953–present
54273	Huadian	Jilin	42.98	126.75	1956–present
54276	Jingyu	Jilin	42.35	126.82	1955–present
54284	Donggang	Jilin	42.10	127.57	1957–present
54285	Songjiang	Jilin	42.53	128.25	1958–present
54287	Tianchi	Jilin	42.02	128.08	1959–present
54292	Yanji	Jilin	42.87	129.50	1953–present
54324	Chaoyang	Liaoning	41.55	120.45	1953–present
54326	Yebaishou	Liaoning	41.38	119.70	1953–present
54335	Heishan	Liaoning	41.68	122.08	1956–present
54337	Jinzhou	Liaoning	41.13	121.12	1951–present
54339	Anshan	Liaoning	41.08	123.00	1951–present
54342	Shenyang	Liaoning	41.73	123.52	1951–present
54346	Benxi	Liaoning	41.32	123.78	1956–present
54351	Zhangdang	Liaoning	41.92	124.08	1951–present
54363	Tonghua	Jilin	41.68	125.90	1951–present
54365	Huanren	Liaoning	41.28	125.35	1953–present
54374	Linjiang	Jilin	41.80	126.92	1953–present
54377	Jianan	Jilin	41.10	126.15	1954–present

TABLE 1: Continued.

WMO number	Station name	Province	Latitude (°N)	Longitude (°E)	Period of operation
54386	Changbai	Jilin	41.42	128.18	1957–present
54454	Suizhong	Liaoning	40.35	120.35	1956–present
54455	Xingcheng	Liaoning	40.58	120.70	1951–present
54471	Yingkou	Liaoning	40.65	122.17	1951–present
54476	Xiongyue	Liaoning	40.17	122.15	1952–present
54486	Xiuyan	Liaoning	40.28	123.28	1953–present
54493	Kuandian	Liaoning	40.72	124.78	1954–present
54497	Dandong	Liaoning	40.05	124.33	1951–present
54563	Wafangdian	Liaoning	39.63	122.02	1957–present
54584	Zhuanghe	Liaoning	39.72	122.95	1956–present
54662	Dalian	Liaoning	38.90	121.63	1951–present

$$\hat{\psi}_0(s\omega) = \pi^{-1/4} H(\omega) e^{-(s\omega - \omega_0)^2/2}, \quad (7)$$

where s represents the wavelet scale; ω means the frequency; $H(\omega)$ is the heaviside step function, $H(\omega) = 1$ if $\omega > 0$, $H(\omega) = 0$ otherwise; and ω_0 means the non-dimensional frequency, thus taken to be 6 to meet the adaptability condition [50].

3. Results and Discussion

3.1. Temporal Variation of Meteorological Variables. The yearly and seasonal average temperature exhibited an increase in Northeast China, at the rate of $0.38^\circ\text{C}/10\text{ yr}$ ($P < 0.01$) in recent 50 years [51], similar to the findings reported by Lu et al. [52]; Li et al. [34], and Zhang et al. [30] in Songhua River Basin, Southwestern China, and Heilongjiang Province. There was a clear decreasing trend in annual precipitation during 1960–2009 in the Songhua River Basin [53]. An obvious peak appeared in July in monthly distribution in Northeast China, and the maximum was 151 mm/month, which is remarkably higher than that occurred in preceding months where the values did not exceed 10 mm/month. Summer precipitation from June to August accounted for about 66% of the total precipitation [54]. The sunshine time and growing season (April to September) presented the declined trend, especially in the Songnen Plain, midwest of Jilin province, and west part of Liaohe Plain in recent decades [31]. Meanwhile, the wind speed and relative humidity likewise presented decreasing trend, and the precipitation as an important climate parameter that influences the ET_0 and AI also decreased during 1965–2017 exhibiting a trend of -0.65 mm/yr .

3.2. Annual Variations of ET_0 and AI. The regional average values of ET_0 in Northeast China during 1965 to 2017 were shown in Figure 2. The average of annual total ET_0 from 1965 to 2017 was 611 mm, and the maximum (680 mm) appeared in 1982 and the minimum appeared in 2017. Linear regression displayed that the annual average ET_0 in the study area presented a decrease trend at a rate of -1.97 mm/yr (Figure 2(a)), and this trend of annual ET_0 was similar to the results obtained in North China and

Pearl River Basin [11, 54, 55]. However, the observed annual ET_0 greatly declined at the rate of -3.09 mm/yr in arid area of Northwest China in the past 54 years [29], and the decline rate was about 1.5 times higher than that estimated in Northeast China. Huo et al. [20] concluded that the contribution of wind speed to the ET_0 decrease was more than that of other meteorological factors in arid area in Northwest China. As mentioned above, the average annual temperature increased over the study region, whereas the annual ET_0 showed a declined trend, suggesting the existence of paradox because an increase in temperature usually leads to upward ET_0 . Nevertheless, effect of increasing temperature was offset by obviously declining the wind speed and relative humidity. For example, both the annual wind speed and relative humidity presented decreasing trends at the rate of $-0.012\text{ m}\cdot\text{s}^{-1}/\text{yr}$ and $-0.05\%/yr$ in the study area, respectively. The correlation coefficient between wind speed and ET_0 was high with a value up to 0.682, followed by relative humidity (0.601) and sunshine duration (0.551), indicating that wind speed and relative humidity were two main climatic factors responsible for the variation of ET_0 in the study region. The precipitation decreased at the rate of 0.65 mm/yr over the study region and was the main meteorological factor resulting in downward AI due to the high correlation coefficient (0.710), which was followed by wind speed (correlation coefficient = 0.583).

Besides, we also investigated the trends of ET_0 in three provinces over Northeast China, including Liaoning, Jilin, and Heilongjiang provinces. The results exhibited that the trend of ET_0 was consistently decreasing with the whole study region, at the rate of -2.50 mm/yr , -1.63 mm/yr , and -1.76 mm/yr , respectively (Figures 2(b)–2(d)). Obviously, the most pronounced decreasing trend occurred in Heilongjiang province over Northeast China, and it has contributed approximately to 42% of ET_0 decrease in Northeast, which had two different phases, mainly divided by the change point in 1989 (Figure 6). The ET_0 was higher during 1961–1989 compared with the entire period and presented the volatile downward trend, whereas ET_0 showed significantly declined trend during 1990–2017. It revealed that Northeast China tended to be wetter in recent two decades. The statistical tendency of annual average AI in Northeast China is shown in Figure 3. The highest AI

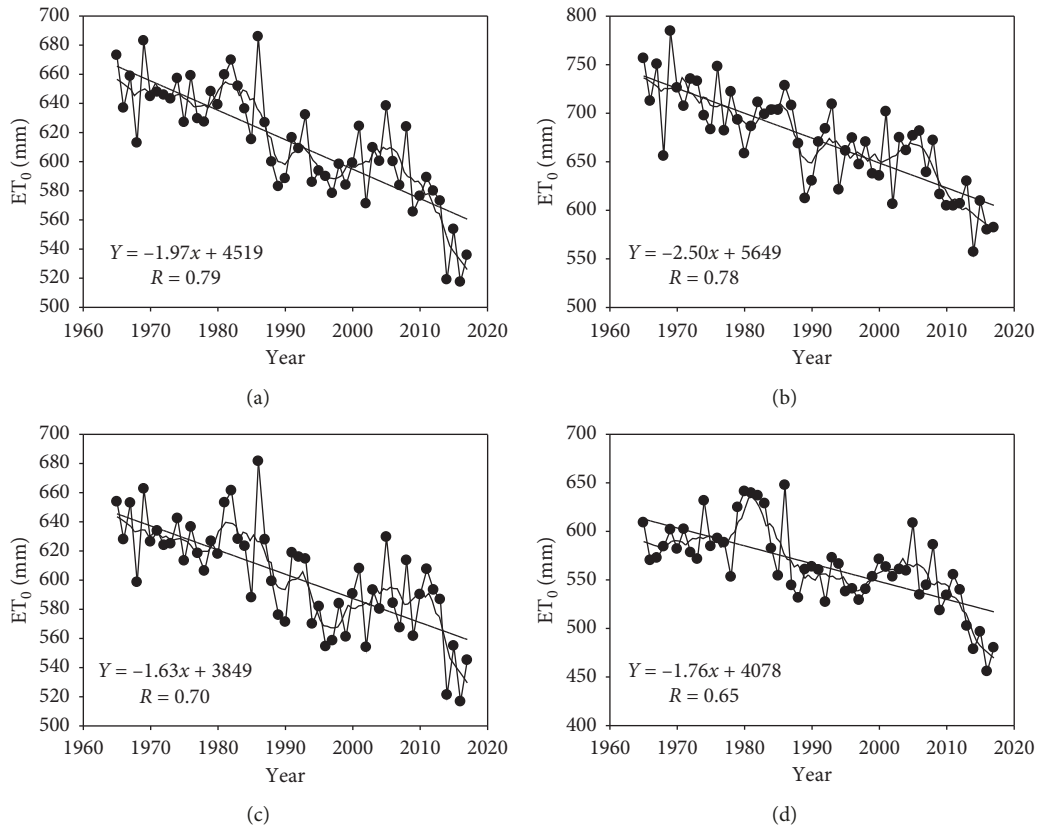


FIGURE 2: Areal average ET_0 changes over Northeast China during 1965–2017. (a) Northeast China. (b) Liaoning. (c) Jilin. (d) Heilongjiang.

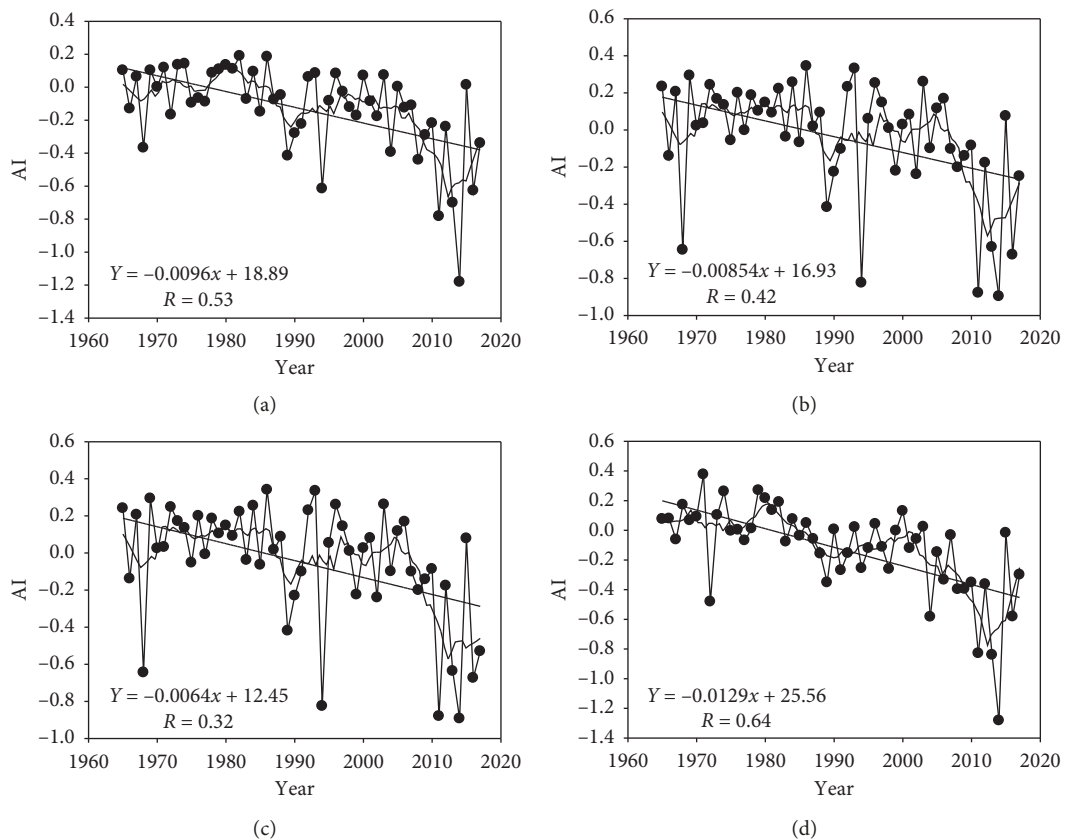


FIGURE 3: Areal average AI changes over Northeast China during 1965–2017. (a) Northeast China. (b) Liaoning. (c) Jilin. (d) Heilongjiang.

value was observed in 1978 (0.19), and the lowest value appeared in 2010 (−1.18). The annual AI had an insignificant declined trend at a rate of about $-0.01/\text{yr}$ from 1965 to 2017, and the linear trend of AI was statistically nonsignificant (Figure 3(a)), as well as the three provinces of Northeast China likewise showed statistically decreased trends at the rate of $-0.0085/\text{yr}$, $-0.0064/\text{yr}$, and $-0.0129/\text{yr}$, respectively. The decline trend rate for Heilongjiang province was the largest of all and contributed to 46% for Northeast China. It was consistent with Northwest China and Loess Plateau region, which implied that Northeast China tended to be wetter; this was probably due to the decrease of annual wind speed, sunshine time, and ET_0 over Northeast China.

3.3. Interdecadal Changes of ET_0 and AI. For the purpose of investigating the temporal variation characteristics in ET_0 and AI in Northeast China during the past 53 years, the interdecadal change trends were analyzed by probability distribution functions (PDFs). Figure 4 displayed the PDFs of the occurrence of annual ET_0 and AI in the past 53 years. The ET_0 presented an increasing trend from the 1960s to the 1970s, then decreased in the 1980s, and displayed a decreasing rapidly trend in 1990s to the period of 2000–2017, which was consistent with previous study results [28]. Moreover, AI exhibited a positive tendency from the 1960s to the 1970s and presented a rapid decreasing trend in 2000s.

3.4. Spatial Distributions of ET_0 and AI. To better understand the spatial distributions of the ET_0 and AI in Northeast China, the Z_c value was calculated by the M-K test. Figures 5(a) and 5(c) display the average value and the tendency of ET_0 and AI over Northeast China from 1965 to 2017. As is shown in Figure 5(a), most stations with high ET_0 were distributed in the west of the study region except for Heilongjiang province, while the stations with low values of ET_0 were primarily located in the central and eastern part. The regions that displayed maximum (814.92/mm) of ET_0 appeared at Chaoyang station in Liaoning province, and the minimum (403.96/mm) appeared in Heihe station, exhibiting large variations in the average value of ET_0 in the study area. The obvious difference between the two stations mentioned above can be mainly attributed to the temperature [56]. These stations with low values of ET_0 were primarily located in mountainous areas and with a high normalized difference vegetation index [57]. Additionally, the estimated ET_0 in Liaoning province was generally much higher than that of the other two provinces. Figure 5(b) presents spatial patterns for the trend of ET_0 over Northeast China during 1965–2017. Remarkably, considerable stations showed a decreasing tendency for ET_0 , and the proportions of meteorological stations with negative trends were approximately 94% (94% statistically significant), which was consistent with the results in Yangtze River Basin and Tibetan Plateau [25, 27]. Moreover, only four meteorological stations exhibited an increasing trend for ET_0 and these four stations primarily

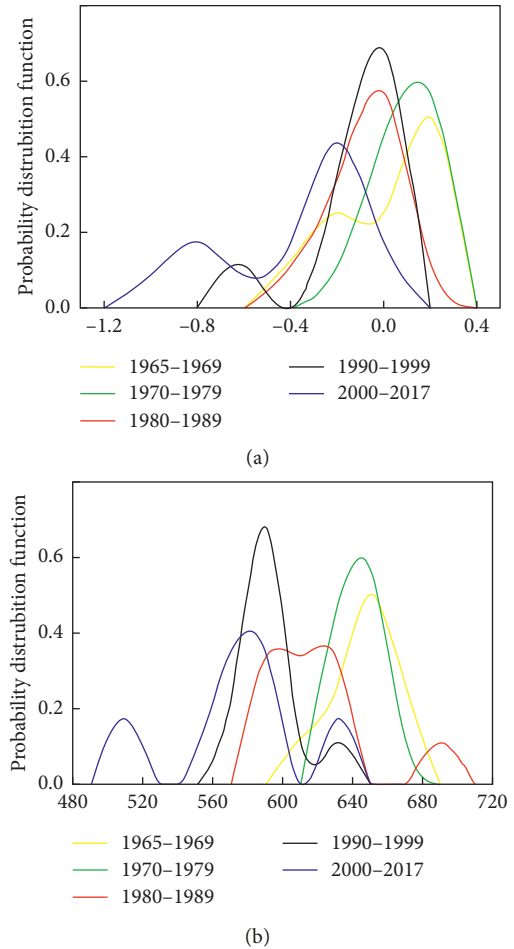


FIGURE 4: Probability distribution functions of precipitation indices in Northeast China during 1965–2017. (a) AI. (b) ET_0 .

distributed in mountain areas in Jilin and Liao provinces, and just one station had shown statistical significant positive trend. Figure 5(c) shows that the distribution of AI stations with higher values was mainly in the western part of Northeast China, which was similar to that of ET_0 , indicating that the western region was dryer than other regions in the study area. The highest value was observed at Tongyu station in Jilin province, and the lowest value was at Kuandian station in Liaoning province. Figure 5(d) shows spatial patterns of trends for AI during 1965–2017, and a large amount of stations presented a decreasing trend for AI on the whole study area. Moreover, around 85% of the stations were at the significant level. Contrarily, only four stations showed an increasing trend with no statistically significant positive trend, the four station mainly in Liaoning and Jilin provinces, and the obtained results was in agreement with the Northwest China [20]. The results suggested Northeast China generally tended to be wetter under global warming, which may be primarily attributed to the topography and increasing vegetation [57].

3.5. Abrupt Change Analysis. Abrupt changes estimated by the M-K method reflected remarkable variation in trends

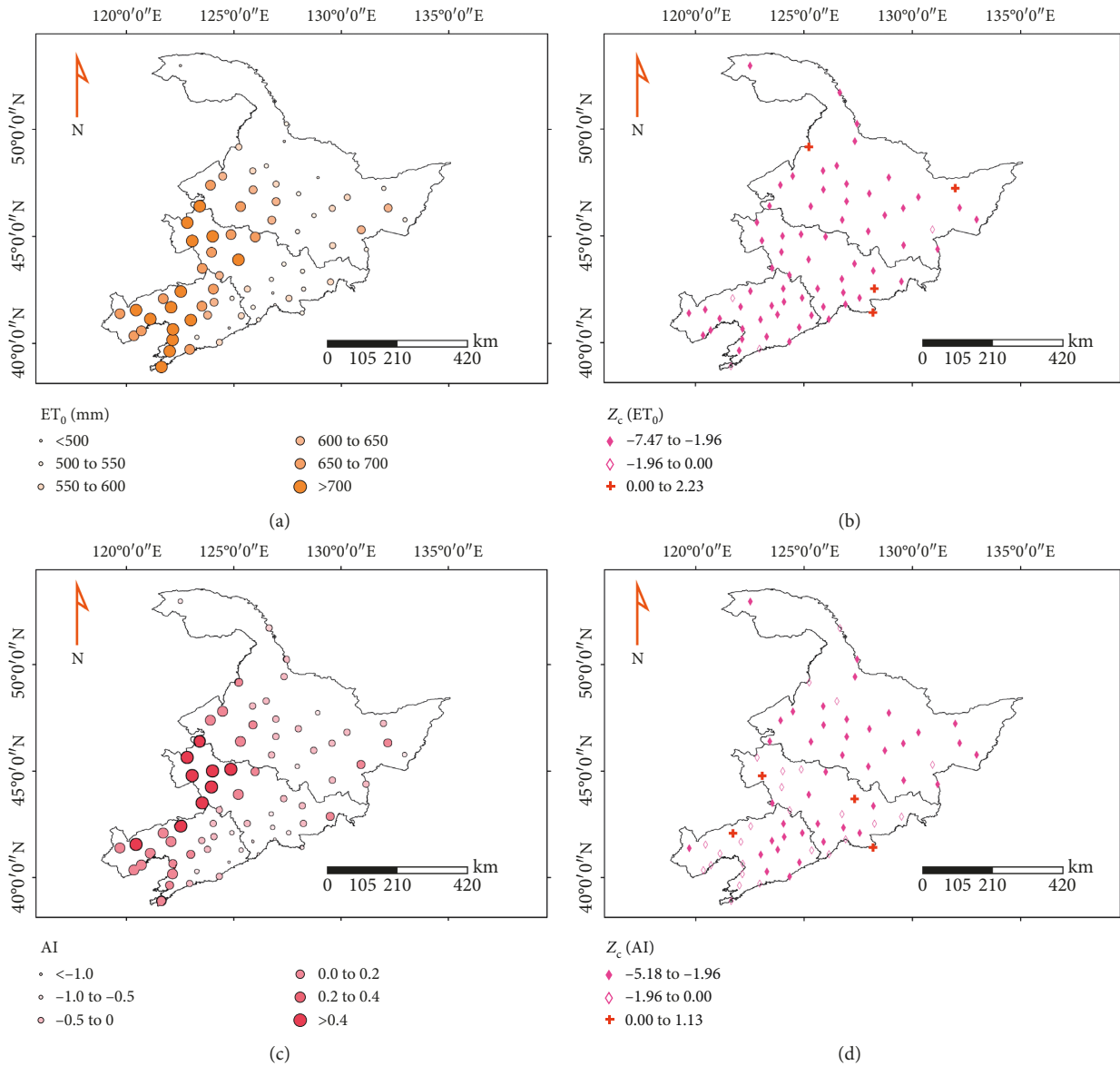


FIGURE 5: Spatial distributions of the M-K test and mean value of ET_0 (a, b) and AI (c, d) over the study area from 1965 to 2017.

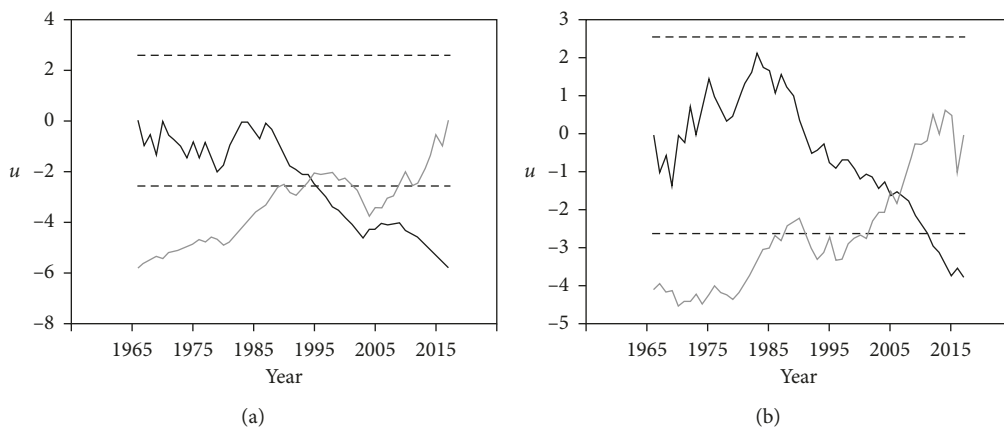


FIGURE 6: M-K analyses of ET_0 (a) and AI (b) over Northeast China. Solid line, C_1 ; gray line, C_2 ; dashed line, significance level at 0.05; the cross point of C_1 and C_2 was the start point in this series.

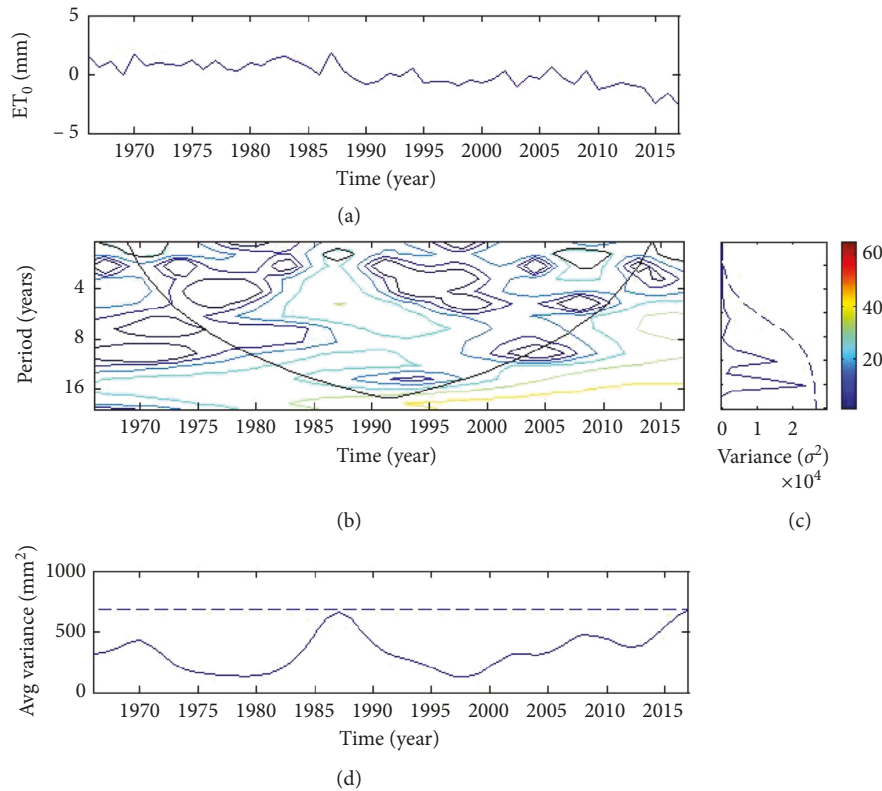


FIGURE 7: Morlet wavelet transformation of annual ET_0 from 1965 to 2017 over Northeast China. (a) The ET_0 time series applied for the wavelet analysis. (b) The local wavelet power spectrum of (a). The thick black contour designates the 5% significance level against red noise and the cone of influence (COI) where edge effects might distort the picture is shown under a thin black curve. (c) Fourier power spectrum of annual ET_0 (solid). The dashed line is the 95% confidence spectrum. (d) Scale-averaged wavelet power over the 2–8 yr band for annual ET_0 (solid). The dashed line is 95% confidence level (The method cite from [35, 49]).

for the target series. Figure 6 shows the test results of ET_0 and AI in Northeast China during 1965–2017. There was only one abrupt change in annual ET_0 , and abrupt point in 1995 was at the 0.01 significance level. The ET_0 showed an interdecadal oscillation before 1995 and then presented a significant declined trend. There were two abrupt changes in the whole change process of time sequence for AI, mainly in 2005 and 2007, significant at 0.01 level. The abrupt change was relatively smaller in 2005, while there was a sudden decline trend, consequently, and thus an abrupt point in 2007 for AI.

3.6. Period Analysis and Climate Teleconnection to the Annual AI. To further estimate the ET_0 and AI variations, we apply the Morlet wavelet transforms to yearly time series of the AI and ET_0 . Figures 7 and 8 show the time-frequency characteristics in real part of the Morlet wavelet method for the ET_0 and AI in Northeast China from 1965 to 2017. In these two figures, (a) represents annual ET_0 time series employed for this analysis. (b) represents local wavelet power spectrums of (a). The black contour designated at 5% significance level against red noise and the cone of influence (COI) is shown using a thin black curve. (c) represents Fourier power spectrums of ET_0 and AI (solid). The dashed line was the 95% confidence spectrum. (d) represents scale-averaged

wavelets over the 2- to 8-year band for ET_0 and AI (solid). The dashed line was at 95% confidence level. For annual ET_0 , it existed periods of 3, 7, 11, and 15 yr that were not significant (Figures 7(b) and 7(c)). There also existed periods of 1, 7, 11, and 13 yr for AI, and only 1 yr period was significant (95% confidence level) (Figures 8(b) and 8(c)). Obviously, the period with significant mean variance of ET_0 was inline with that of AI.

Large-scale climate oscillations play vital roles in regional climate change and water resource cycling. So, it was significant to clarify if the AI and ET_0 had relationship with the MEI, PDO, WNPPI, and ISMI. Thus, these correlation coefficients among indexes mentioned above were analyzed. As shown in Figure 9, obviously, the MEI, PDO, WNPPI, and ISMI were all positively correlated with AI. These selected indexes displayed increasing trends in Northeast China during the 1965–2017. Overall, the increasing trend for AI with ISMI was the most remarkable of all the indexes and significant at the 0.05 level, which suggested a remarkable impact of the ISMI on AI. The lower R values were presented between AI and MEI, PDO, and WNPPI, indicating that the effect of the three selected indexes on AI was not significant. In recent decades, climatic anomaly and extreme climatic event in Asia [2] may affect the correlation between AI and the indexes. However, apart from the climate elements and natural oscillations, anthropogenic

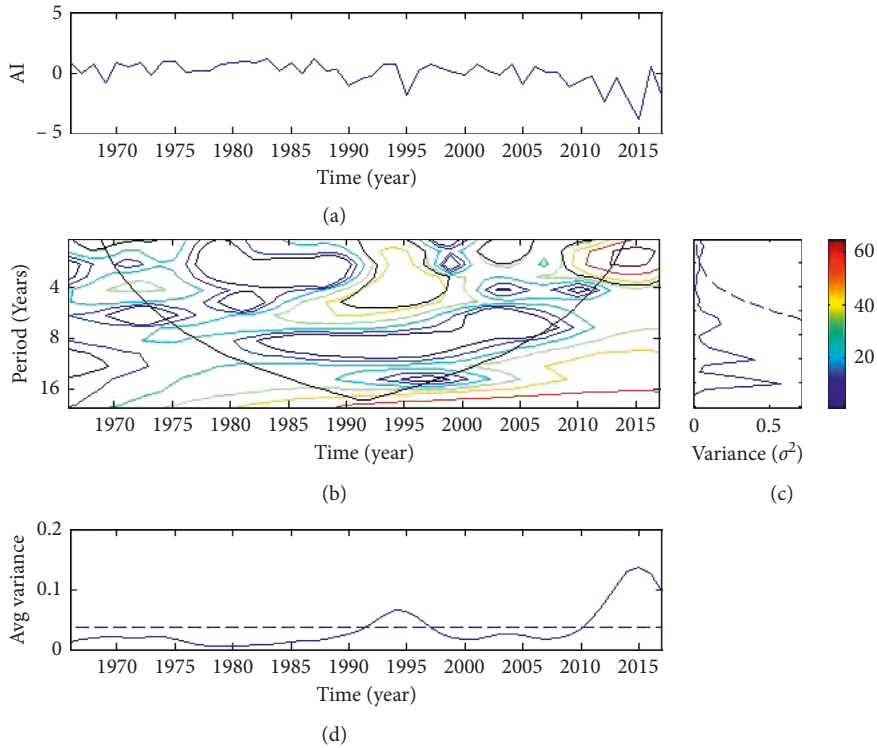


FIGURE 8: Morlet wavelet transformation of annual AI from 1965 to 2017 over Northeast China. (a) The annual ET₀ time series used for the wavelet analysis. (b) The local wavelet power spectrum of (a). The thick black contour designates the 5% significance level against red noise and the cone of influence (COI) where edge effects might distort the picture is shown under a thin black curve. (c) Fourier power spectrum of annual ET₀ (solid). The dashed line is the 95% confidence spectrum. (d) Scale-averaged wavelet power over the 2–8 yr band for annual ET₀ (solid). The dashed line is 95% confidence level (the method is cited from [35, 49]).

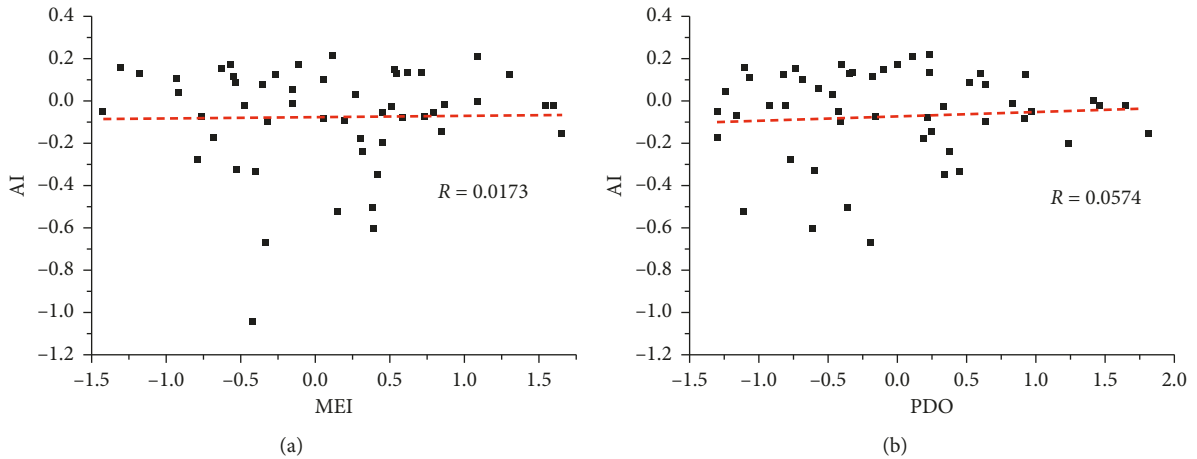


FIGURE 9: Continued.

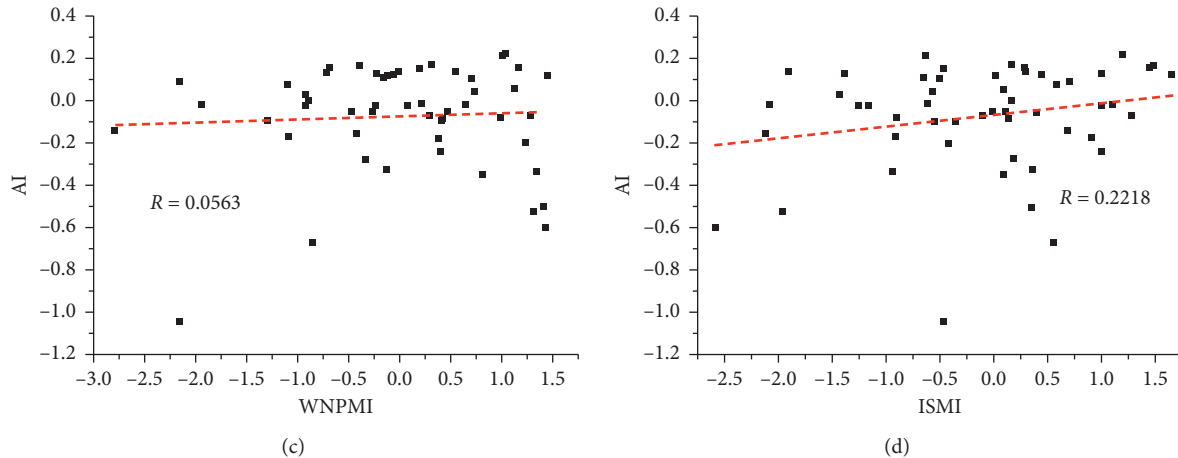


FIGURE 9: Correlation between AI and MEI, PDO, WNPMI, and ISMI from 1965 to 2017 period, respectively.

forcing induced by human activities should be paid attention as well [58, 59]. Besides, deforestation and urbanization are also potential factors that influence the AI. Therefore, it remains a long way to go for adequate understanding of the influence of climate oscillations, meteorological factors and human activities on AI as well as ET_0 , which needs further investigation in the ongoing research.

4. Conclusions

According to the collected dataset from 71 meteorological stations over Northeast China from 1965 to 2017, the spatial and temporal variations of the AI and ET_0 were investigated. The average of annual total ET_0 was 611.43 mm between 1965 and 2017, presenting a decreased trend of -1.97 mm/yr. The trends of ET_0 across all the observatories exhibited similar decreasing trends, at the rates of -2.50 mm/yr, -1.63 mm/yr, and -1.76 mm/yr, respectively. Annual AI also showed nonsignificant slightly declined trends, at a rate of about -0.01 /yr during 1965–2017; the decline rate of Heilongjiang province was the largest of all and contributed to 46% for Northeast China. The analysis of PDFs indicated that the ET_0 has an increasing trend from 1960s to 1970s and then decreased in the 1980s, as well as it displayed a rapidly decreasing trend in 1990s to the period of 2000–2017. AI showed a positive tendency from the 1960s to the 1970s but displayed a rapid decrease in 2000s. Considerable stations with high values of ET_0 were mainly in the western part of the study area except for Heilongjiang province, and most stations with low values were primarily suited in the central and eastern part, which was generally consistent with the AI over the study area. Moreover, there were two abrupt changes in the whole change process of time sequence for AI, primarily in 2005 and 2007, and abrupt point of ET_0 happened in 1995. There were periods of 3, 7, 11, and 15 yr that were nonsignificant trends. Meanwhile, there existed periods of 1, 7, 11, and 13 yr, for AI, and 1 yr period that was significant at 95% confidence level. Consequently, the results of this research estimated climate drought over past decades and addressed

the possible causes. However, further investigation is still required to clarify the mechanisms of variability in AI and ET_0 over Northeast China in the future.

Data Availability

The data used to support the findings of this study are available from the corresponding author upon request.

Conflicts of Interest

The authors declare that they have no conflicts of interest.

Acknowledgments

This work was partially supported by the National Key Research and Invention Program of the Thirteenth (2017YFC0504702); The Science and Technology Service Network Initiative Project of Chinese Academy of Sciences (KFJ-STZ-ZDTP-036); National Natural Science Funds of China (41771220); Natural Science Foundation of Shaanxi Province (2018JM4020); The Fundamental Research Funds for the Central Universities (GK201803047, GK201903075, GK201703051, GK201903071).

References

- [1] IPCC, "Climate change: impacts, adaptation, and vulnerability. Summary for policymakers," Report of Working Group II of the Intergovernmental Panel on Climate Change, Cambridge University Press, Cambridge, UK, 2007.
- [2] IPCC, *Climate Change: The Physical Science Basis*, Cambridge University Press, Cambridge, UK, 2013, <http://www.ipcc.ch/report/ar5/wg1#.Uq-tD7K%20BRRL>.
- [3] D. R. Easterling, J. L. Evans, P. Y. Groisman, T. R. Karl, K. E. Kunkel, and P. Ambenje, "Observed variability and trends in extreme climate events: a brief review," *Bulletin of the American Meteorological Society*, vol. 81, no. 3, pp. 417–425, 2000.
- [4] J. T. Houghton, Y. Ding, J. Griggs et al., "Climate change 2001: the scientific basis. Observed climate variability and change," in *Contribution of Working Group I to the Third Assessment*

- Report of the Intergovernmental Panel on Climate Change*, pp. 1–881, Cambridge University Press, Cambridge, UK, 2001.
- [5] Q. Zhang, J. Li, X. Gu, and P. Shi, “Is the Pearl River basin, China, drying or wetting? Seasonal variations, causes and implications,” *Global and Planetary Change*, vol. 166, pp. 48–61, 2018.
- [6] E. Aguilar, A. Barry, M. Brunet et al., “Changes in temperature and precipitation extremes in western central Africa, Guinea Conakry, and Zimbabwe, 1955–2006,” *Journal of Geophysical Research*, vol. 114, no. D2, 2009.
- [7] E. E. Houssos, C. J. Lolis, and A. Bartzokas, “Atmospheric circulation patterns associated with extreme precipitation amounts in Greece,” *Advances in Geosciences*, vol. 17, pp. 5–11, 2008.
- [8] A. Tall, A. G. Patt, and S. Fritz, “Reducing vulnerability to hydro-meteorological extremes in Africa. A qualitative assessment of national climate disaster management policies: accounting for heterogeneity,” *Weather and Climate Extremes*, vol. 1, pp. 4–16, 2013.
- [9] L. Cao, S. Pan, Q. Wang, Y. Wang, and W. Xu, “Changes in extreme wet events in Southwestern China in 1960–2011,” *Quaternary International*, vol. 321, pp. 116–124, 2014.
- [10] N. Endo, J. Matsumoto, and T. Lwin, “Trends in precipitation extremes over southeast Asia,” *SOLA*, vol. 5, pp. 168–171, 2009.
- [11] Y. Zhao, X. Zou, L. Cao, and X. Xu, “Changes in precipitation extremes over the Pearl River basin, southern China, during 1960–2012,” *Quaternary International*, vol. 333, pp. 26–39, 2014.
- [12] K.-X. Zhang, S.-M. Pan, W. Zhang et al., “Influence of climate change on reference evapotranspiration and aridity index and their temporal-spatial variations in the Yellow River Basin, China, from 1961 to 2012,” *Quaternary International*, vol. 380–381, pp. 75–82, 2015.
- [13] I. Kioutsioukis, D. Melas, and C. Zerefos, “Statistical assessment of changes in climate extremes over Greece (1955–2002),” *International Journal of Climatology*, vol. 30, no. 11, pp. 1723–1737, 2010.
- [14] O. Zolina, C. Simmer, A. Kapala, S. Bachner, S. Gulev, and H. Maechel, “Seasonally dependent changes of precipitation extremes over Germany since 1950 from a very dense observational network,” *Journal of Geophysical Research*, vol. 113, no. D6, 2008.
- [15] M. R. Haylock, T. C. Peterson, L. M. Alves et al., “Trends in total and extreme South American rainfall in 1960–2000 and links with sea surface temperature,” *Journal of Climate*, vol. 19, no. 8, pp. 1490–1512, 2006.
- [16] G. Kuhn, S. Khan, A. R. Ganguly, and M. L. Branstetter, “Geospatial-temporal dependence among weekly precipitation extremes with applications to observations and climate model simulations in South America,” *Advances in Water Resources*, vol. 30, no. 12, pp. 2401–2423, 2007.
- [17] H. F. Blaney and W. D. Criddle, “Determining water requirements in irrigated area from climatological irrigation data,” Technical Paper No. 96, US Department of Agriculture, Soil Conservation Service, 1950.
- [18] Z. Wang, P. Xie, C. Lai et al., “Spatiotemporal variability of reference evapotranspiration and contributing climatic factors in China during 1961–2013,” *Journal of Hydrology*, vol. 544, pp. 97–108, 2017.
- [19] C.-Y. Xu and V. P. Singh, “Evaluation of three complementary relationship evapotranspiration models by water balance approach to estimate actual regional evapotranspiration in different climatic regions,” *Journal of Hydrology*, vol. 308, no. 1–4, pp. 105–121, 2005.
- [20] Z. Huo, X. Dai, S. Feng, S. Kang, and G. Huang, “Effect of climate change on reference evapotranspiration and aridity index in arid region of China,” *Journal of Hydrology*, vol. 492, pp. 24–34, 2013.
- [21] A. Thomas, “Spatial and temporal characteristics of potential evapotranspiration trends over China,” *International Journal of Climatology*, vol. 20, no. 4, pp. 381–396, 2000.
- [22] M. T. Hobbins, J. A. Ramirez, and T. C. Brown, “Trends in pan evaporation and actual evapotranspiration across the conterminous U.S.: paradoxical or complementary?,” *Geophysical Research Letters*, vol. 31, no. 13, 2004.
- [23] T. C. Peterson, V. S. Golubev, and P. Y. Groisman, “Evaporation losing its strength,” *Nature*, vol. 377, no. 6551, pp. 687–688, 1995.
- [24] D. W. Yang, F. B. Sun, Z. Y. Liu, Z. T. Cong, and Z. D. Lei, “Interpreting the complementary relationship in non-humid environments based on the Budyko and Penman hypotheses,” *Geophysical Research Letters*, vol. 33, no. 18, pp. 1–5, 2006.
- [25] L. Liang, L. Li, and Q. Liu, “Temporal variation of reference evapotranspiration during 1961–2005 in the Taoer River basin of Northeast China,” *Agricultural and Forest Meteorology*, vol. 150, no. 2, pp. 298–306, 2010.
- [26] Y. Wang, T. Jiang, O. Bothe, and K. Fraedrich, “Changes of pan evaporation and reference evapotranspiration in the Yangtze River basin,” *Theoretical and Applied Climatology*, vol. 90, no. 1–2, pp. 13–23, 2007.
- [27] Y. Q. Zhang, C. M. Liu, and Y. H. Tang, “Trends in pan evaporation and reference and actual evapotranspiration across the Tibetan Plateau,” *Journal of Geophysical Research*, vol. 112, pp. 1–12, 2007.
- [28] L. Wang, L. Cao, X. Deng et al., “Changes in aridity index and reference evapotranspiration over the central and eastern Tibetan Plateau in China during 1960–2012,” *Quaternary International*, vol. 349, pp. 280–286, 2014.
- [29] D. Z. Ye, *China’s Global Change Research Advance (Part II)*, Seismological Press, Beijing, China, 1994, in Chinese.
- [30] Q. Zhang, C. Liu, C.-Y. Xu, Y. Xu, and T. Jiang, “Observed trends of annual maximum water level and streamflow during past 130 years in the Yangtze River basin, China,” *Journal of Hydrology*, vol. 324, no. 1–4, pp. 255–265, 2006.
- [31] Z. J. Liu, X. G. Yang, W. F. Wang, K. N. Li, and X. Y. Zhang, “Characteristics of agricultural climate resources in three provinces of Northeast China under global climate change,” *Chinese Journal of Applied Ecology*, vol. 20, pp. 2199–2206, 2009, in Chinese.
- [32] R. G. Allen, L. S. Pereira, D. Raes, and M. Smith, *Crop Evapotranspiration Guidelines for Computing Crop Water Requirements*, FAO Irrigation and Drainage Paper 56, Rome, Italy, 1998.
- [33] Z. Li, Y. He, W. An et al., “Climate and glacier change in southwestern China during the past several decades,” *Environmental Research Letters*, vol. 6, no. 4, article 045404, 2011.
- [34] Z. X. Li, Y. Q. He, P. Y. Wang et al., “Changes of daily climate extremes in southwestern China during 1961–2008,” *Global Planet Change*, vol. 80–81, pp. 255–272, 2012.
- [35] Y. Zhao, X. Zou, J. Zhang et al., “Spatio-temporal variation of reference evapotranspiration and aridity index in the Loess Plateau Region of China, during 1961–2012,” *Quaternary International*, vol. 349, pp. 196–206, 2014.
- [36] S. ChenZhang, W. D. Graham, and J. M. Jacobs, “Daily potential evapotranspiration and diurnal climate forcings: influence on the numerical modelling of soil water dynamics

- and evapotranspiration,” *Journal of Hydrology*, vol. 309, no. 1–4, pp. 39–52, 2005.
- [37] C. W. Thornthwaite, “An approach toward a rational classification of climate,” *Geographical Review*, vol. 38, no. 1, pp. 57–94, 1948.
- [38] M. G. Kendall, *Rank Correlation Methods*, Charles Griffin, London, UK, 1975.
- [39] H. B. Mann, “Nonparametric tests against trend,” *Econometrica*, vol. 13, no. 3, pp. 245–259, 1945.
- [40] J. M. Mitchell, B. Dzerdzeevskii, H. Flohn et al., “Climatic change,” WMO Technical Note No. 79, World Meteorological Organization, Geneva, Switzerland, 1966.
- [41] P.-S. Yu, T.-C. Yang, and C.-K. Wu, “Impact of climate change on water resources in southern Taiwan,” *Journal of Hydrology*, vol. 260, no. 1–4, pp. 161–175, 2002.
- [42] K. H. Hamed, “Trend detection in hydrologic data: the Mann-Kendall trend test under the scaling hypothesis,” *Journal of Hydrology*, vol. 349, no. 3–4, pp. 350–363, 2008.
- [43] S. W. Zhang, Y. Z. Zhang, Y. Li, and L. P. Chang, *Temporal and Spatial Variations of Land Use/Cover Changes in Northeast China*, Sciences Press, Beijing, China, 2006, in Chinese.
- [44] Q. Zhang, C.-Y. Xu, and Z. Zhang, “Observed changes of drought/wetness episodes in the Pearl River basin, China, using the standardized precipitation index and aridity index,” *Theoretical and Applied Climatology*, vol. 98, no. 1–2, pp. 89–99, 2009.
- [45] W. Zhang, S. Pan, L. Cao et al., “Changes in extreme climate events in eastern China during 1960–2013: a case study of the Huaihe River Basin,” *Quaternary International*, vol. 380–381, pp. 22–34, 2015.
- [46] L. S. Ren, S. Wang, and X. Fan, “Channel change at Tou-daoguai Station and its responses to the operation of upstream reservoirs in the upper Yellow River,” *Journal of Geographical Sciences*, vol. 20, no. 2, pp. 231–247, 2010.
- [47] C. Torrence and G. P. Compo, “A practical guide to wavelet analysis,” *Bulletin of the American Meteorological Society*, vol. 79, no. 1, pp. 61–78, 1998.
- [48] H. EL-Askary, S. Sarkar, L. Chiu, M. Kafatos, and T. El-Ghazawi, “Rain gauge derived precipitation variability over Virginia and its relation with the El Nino southern oscillation,” *Advances in Space Research*, vol. 33, no. 3, pp. 338–342, 2004.
- [49] N. R. Rigozo, D. J. R. Nordemann, E. Echer, A. Zanandrea, and W. D. Gonzalez, “Solar variability effects studied by tree-ring data wavelet analysis,” *Advances in Space Research*, vol. 29, no. 12, pp. 1985–1988, 2002.
- [50] M. Farge, “Wavelet transforms and their applications to turbulence,” *Annual Review of Fluid Mechanics*, vol. 24, no. 1, pp. 395–457, 1992.
- [51] W. He, R. C. Bu, Z. P. Xiong, and Y. M. Hu, “Characteristics of temperature and precipitation in Northeastern China from 1961 to 2005,” *Acta Ecologica Sinica*, vol. 33, pp. 0519–0531, 2013, in Chinese.
- [52] Z. H. Lu, Z. Q. Xia, L. L. Yu, and J. C. Wang, “Characteristics of spatio-temporal variation of temperature in Songhua River basin from 1960 to 2010,” *Journal of Hohai University*, vol. 40, pp. 629–635, 2012, in Chinese.
- [53] F. Li, G. Zhang, and Y. J. Xu, “Spatiotemporal variability of climate and streamflow in the Songhua River Basin, northeast China,” *Journal of Hydrology*, vol. 514, pp. 53–64, 2014.
- [54] G. Gao, D. L. Chen, G. Y. Ren, Y. Chen, and Y. M. Liao, “Trend of potential evapotranspiration over China during 1956 to 2000,” *Geographical Research*, vol. 25, no. 3, pp. 378–387, 2006, in Chinese.
- [55] X. Q. Xie and L. Wang, “Changes of potential evaporation in northern China over the past 50 years,” *Journal of Natural Resources*, vol. 22, no. 5, pp. 683–691, 2007, in Chinese.
- [56] H. S. Pan, G. H. Zhang, and N. P. Xu, “A preliminary analysis of climate warming in Heilongjiang province since the 1980s,” *Climatic and Environmental Research*, vol. 8, no. 3, pp. 343–355, 2003, in Chinese.
- [57] Q. Wang, B. Zhang, Z. Q. Zhang, X. F. Zhang, and S. P. Dai, “The three-North Shelterbelt Program and dynamic changes in vegetation cover,” *Journal of Resources and Ecology*, vol. 5, no. 1, pp. 53–59, 2014.
- [58] W. Zhang and B. Kirtman, “Estimates of decadal climate predictability from an interactive ensemble model,” *Geophysical Research Letters*, vol. 46, no. 6, pp. 3387–3397. In press, 2019.
- [59] L. Liang, L. Li, and Q. Liu, “Precipitation variability in northeast China from 1961 to 2008,” *Journal of Hydrology*, vol. 404, no. 1–2, pp. 67–76, 2011.



Hindawi

Submit your manuscripts at
www.hindawi.com

